

High-precision three-dimensional atom localization via probe absorption at room temperature

Mengmeng Luo(罗萌萌), Wenxiao Liu(刘文晓), Dingyu Cai(蔡定宇), and Shaoyan Gao(高韶燕)

Citation: Chin. Phys. B, 2020, 29 (**12**): 124205. DOI: 10.1088/1674-1056/abb3df
Journal homepage: http://cpb.iphy.ac.cn; http://iopscience.iop.org/cpb

What follows is a list of articles you may be interested in

Effect of residual Doppler averaging on the probe absorption in cascade type system: A comparative study

Suman Mondal, Arindam Ghosh, Khairul Islam, Dipankar Bhattacharyya, Amitava Bandyopadhyay
Chin. Phys. B, 2018, 27 (**9**): 094204. DOI: 10.1088/1674-1056/27/9/094204

Analytical solutions for a doubly driven two-level atom

Jin-Yun Liu(刘晋允), Feng-Dong Jia(贾凤东), Xiao-Kang Li(李晓康), Shuang-Fei Lv(吕双飞), Xiang-Yuan Xu(许祥源), Ping Xue(薛平), Zhi-Ping Zhong(钟志萍)
Chin. Phys. B, 2017, 26 (**7**): 074203. DOI: 10.1088/1674-1056/26/7/074203

r^{3+} ion concentration effect on transient and steady-state behaviorin Er^{3+} ： YAG crystal

Asadpour Seyyed Hossein, Rahimpour Soleimani H
Chin. Phys. B, 2014, 23 (**10**): 104223. DOI: 10.1088/1674-1056/23/10/104223

Two-dimensional atom localization via probe absorption in a four-level atomic system

Wang Zhi-Ping, Ge Qiang, Ruan Yu-Hua, Yu Ben-Li
Chin. Phys. B, 2013, 22 (**7**): 074203. DOI: 10.1088/1674-1056/22/7/074203

High-precision two-dimensional atom localization via probe absorption in M-scheme atomic system

Wu Jian-Chun, Liu Zheng-Dong, Zheng Jun
Chin. Phys. B, 2013, 22 (**4**): 044203. DOI: 10.1088/1674-1056/22/4/044203

High-precision three-dimensional atom localization via probe absorption at room temperature

Mengmeng Luo(罗萌萌), Wenxiao Liu(刘文晓), Dingyu Cai(蔡定宇), and Shaoyan Gao(高韶燕)†

MOE Key Laboratory for Nonequilibrium Synthesis and Modulation of Condensed Matter, Shaanxi Province Key Laboratory of Quantum Information and Quantum Optoelectronic Devices, School of Physics, Xi'an Jiaotong University, Xi'an 710049, *China*

(Received 29 May 2020; revised manuscript received 20 July 2020; accepted manuscript online 1 September 2020)

A scheme is used to explore the behavior of three-dimensional (3D) atom localization in a Y-type hot atomic system. We can obtain the position information of the atom due to the position-dependent atom–field interaction. We study the influences of the system parameters and the temperature on the atom localization. More interestingly, the atom can be localized in a subspace when the temperature is equal to 323 K. Moreover, a method is proposed to tune multiparameter for localizing the atom in a subspace. The result is helpful to achieve atom nanolithography, photonic crystal and measure the center-of-mass wave function of moving atoms.

Keywords: three-dimensional atom localization, probe absorption, Doppler effect

PACS: 42.50.−p, 42.50.Gy, 43.30.Es **DOI:** 10.1088/1674-1056/abb3df

1. Introduction

New physical effects or natural laws will be found when the effective number of the measured physical variable increases by an order of magnitude. In other words, modern physics is developed in the pursuit of high precision. Achieving high-precision atom localization is an important part of precise measurement physics. Atom localization has lots of potential applications in laser cooling and trapping of neutral atoms,[1,2] quantum information science,[3] coherent patterning of matter waves,[4] the measurement of the center-of-mass wave function of moving atoms,[5,6] atom nanolithography,[7] and Bose–Einstein condensation.[8–10] The diffractive scattering always occurs when the atom interacts with a periodic structure of light. Thus, it is difficult to realize the precision of atom localization that is better than the wavelength of the applied light beam.[11] However, some approaches have gone beyond this limit, such as the measurement of the atomic dipole,[12] the phase shift of the standing-wave field,[13–15] the atomic resonance frequency,[16–18] and so on. As an important quantum effect, electromagnetically induced transparency, which makes possible to achieve the high-precision atom localization, attracts many attention of researchers.[19–23]

During the past few decades, a number of schemes have come forward for one-dimensional (1D) atom localization by means of quantum interference or atomic coherence effects.[24–34] All these schemes have employed standing-wave driving fields to encode position information into the intensity pattern with the position-dependent Rabi frequency. Afterwards, two-dimensional (2D) atom localization has been extensively studied through applying two orthogonal standing-wave laser fields. The measurements of the controlled spontaneous emission,[35] the upper-level population,[36] and double-dark resonances[37] are used to achieve 2D atom localization. Several schemes for realizing high-resolution and high-precision 2D atom localization have been proposed[38–46] in different atomic systems. Owing to the position-dependent atom–field interaction, we can obtain the position information of the atom by measuring the absorption of the probe field.[47,48] Recently, Song *et al.* found that the atom can be localized in a subspace of the three-dimensional (3D) space and a maximal resolution of $\sim 0.04\lambda$ can be achieved by properly varying the parameters of the system.[49] Zhu *et al.* have achieved high-precision 3D atom localization via three-wave mixing (TWM) in a V-type atomic system.[50] Based on the absorption measurement of a probe field, a scheme of phase-sensitive 3D atom localization has been presented in a driven four-level atomic system with two-fold lower levels and some charming polyhedron-, wave-, bowling-pin-, and tetrahedron-like localization structures have emerged.[51] The above studies remind us of an important question: Is it possible to realize subwavelength atom localization at room temperature?

Ding *et al.* proposed a scheme for achieving high-precision 2D atom localization in a microwave-driven four-level atomic system.[40] Afterwards, Mao *et al.* found that the atom can be localized in a subspace of the 3D space by using the same atomic system when three orthogonal standing-wave fields couple one atomic transition.[52] However, all of them used cold atoms.[40,52] In this paper, we apply a Y-type atomic system for realizing a high-precision 3D atom localization via probe absorption at room temperature. Two cases are considered, one is that three orthogonal standing-wave fields couple different atomic transitions, the other is that three orthogonal standing-wave fields couple one atomic transition. The atom

†Corresponding author. E-mail: gaosy@xjtu.edu.cn

© 2020 Chinese Physical Society and IOP Publishing Ltd

can be localized in a subspace when the temperature is equal to 323 K, to the best of our knowledge, which has not been reported before. We also solve the problem how to tune multiparameter in atom–field interaction.

The rest of this paper is organized as follows. In Section 2, We demonstrate the atomic system and derive the conditional position probability distribution of the atom under the interaction of the atom with a microwave field, a probe field, and three orthogonal standing-wave fields. In Section 3, we give the method applied to tune multiparameter for localizing the atom. We then show and discuss the numerical results of 3D atom localization. Finally, our conclusions are summarized in Section 4.

2. The model and dynamic equations

In Fig. 1, we show the schematic of a four-level Y-type atom with a ground level $|0\rangle$, one intermediate level $|1\rangle$, and two excited levels $|2\rangle$, $|3\rangle$. To measure the probe absorption, a probe laser field $E_{\rm p}$ with a Rabi frequency $2\Omega_{\rm p}$ and a carrier frequency $\omega_{\rm p}$ is used to tune the transition $|0\rangle \leftrightarrow |1\rangle$. Two coherent laser fields with Rabi frequencies Ω_1 and Ω_2 are simultaneously applied to drive the transitions from level $|1\rangle$ to the excited levels $|2\rangle$ and $|3\rangle$, respectively. The two hyperfine levels $|2\rangle$ and $|3\rangle$ are resonantly coupled by an extra microwave-driven field with a Larmor frequency $2\Omega_{\rm mw}$. We will analyze two cases. The first one is that both $G_1(x,y,z)$ and $G_2(x,y,z)$ are the standing-wave fields. The $G_1(x,y,z)$ is combined by two orthogonal standing-wave fields with the same frequency coupled to the transition $|1\rangle \leftrightarrow |2\rangle$, but the $G_2(x,y,z)$ is the standing-wave field coupled to the transition $|1\rangle \leftrightarrow |3\rangle$ in the z direction, i.e., $G_1(x,y,z) = \Omega_1[\sin(k_1x) + \sin(k_1y)]$ and $G_2(x,y,z) = \Omega_2 \sin(k_2z)$, where k_1 and k_2 are the wave vectors of the standing-wave fields. The other case is that the $G_1(x,y,z)$ is combined by three orthogonal standing-wave fields, but the $G_2(x,y,z)$ corresponds to a traveling-wave field, namely, $G_2(x,y,z) = \Omega_2$, respectively. It is worth mentioning that an atom moves through in the z direction. Therefore, the atom will interact with the three orthogonal standing-wave fields. Here we assume that the center-of-mass position of the atom along the direction of the standing-wave fields is nearly constant and we can neglect the kinetic part of the atom in the Hamiltonian by applying the Raman–Nath approximation.[53] Under the rotation-wave approximation (RWA) and the electric dipole approximation (EDA), the interaction Hamiltonian of the atomic system can be written as

$$\begin{aligned} H/\hbar = &-\Delta_{\rm p}|1\rangle\langle 1| - (\Delta_{\rm p}+\Delta_1)|2\rangle\langle 2| - (\Delta_{\rm p}+\Delta_2)|3\rangle\langle 3| \\ &+ [\Omega_{\rm p}|0\rangle\langle 1| + G_1(x,y,z)|1\rangle\langle 2| + G_2(x,y,z)|1\rangle\langle 3| \\ &+ \Omega_{\rm mw}|2\rangle\langle 3| + {\rm H.c.}], \end{aligned} \tag{1}$$

where the symbol H.c. stands for the Hermitian conjugate. The quantities Δ_1, Δ_2, and $\Delta_{\rm p}$ are the relevant frequency detunings of the standing-wave field and the probe field away from the corresponding atomic resonance transition frequencies, respectively. In addition, $\Omega_{\rm mw}$ and $\Omega_{\rm p}$ represent the one-half Larmor and Rabi frequencies of relevant transitions, i.e., $\Omega_{\rm mw} \equiv \mu_{32}B_{\rm mw}/(2\hbar)$ and $\Omega_{\rm p} \equiv \mu_{10}Ep/(2\hbar)$, with $\mu_{jk} = \boldsymbol{\mu}_{jk} \cdot \boldsymbol{e}_L$ ($j,k = 0$–3; $\boldsymbol{e}_L$ is the unit polarization vector of the corresponding laser field) being the dipole moment of the transition $|j\rangle \leftrightarrow |k\rangle$. The dynamics of this system can be described by the corresponding density matrix approach as

$$\dot{\rho} = -\frac{\rm i}{\hbar}[H,\rho] - \frac{1}{2}\{\Gamma,\rho\}, \tag{2}$$

where $\{\Gamma,\rho\} = \Gamma\rho + \rho\Gamma$. A relaxation matrix Γ defined by $\langle n|\Gamma|m\rangle = \gamma_n\delta_{nm}$ gives the decay rate. Substituting the interaction Hamiltonian (1) into Eq. (2), we can derive the equations of density-matrix elements.

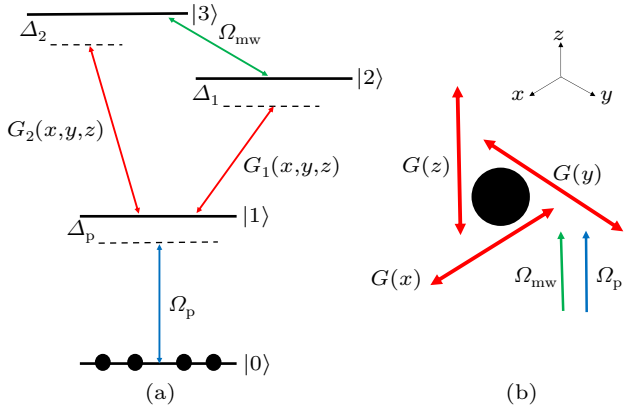


Fig. 1. (a) Schematic diagram of a four-level Y-type atomic system, which consists of a ground level $|0\rangle$, an intermediate level $|1\rangle$, and two excited levels $|2\rangle$ and $|3\rangle$. In the diagram given above, $G_1(x,y,z)$ is a standing-wave field, and $G_2(x,y,z)$ is a standing-wave or traveling-wave field. $2\Omega_{\rm mw}$ is the Larmor frequency for the transition between levels $|2\rangle$ and $|3\rangle$. $\omega_{\rm p}$ is the one-half Rabi frequency of a probe laser field applied to couple levels $|0\rangle$ and $|1\rangle$, while $\Delta_{\rm p}$ is the frequency detuning of the probe laser field. Δ_1 and Δ_2 stand for the frequency detunings of the standing wave or traveling wave fields. All parameters are in units of γ. (b) Three orthogonal standing wave fields $G(x)$, $G(y)$, and $G(z)$ corresponding to the x, y, and z directions form a 3D space, while the probe field $\Omega_{\rm p}$ and the microwave field $\Omega_{\rm mw}$ propagate along the z direction.

The density matrix equations will be calculated by using the weak field approximation since the probe field intensity is weak enough. Then the density-matrix equations can be solved by applying the perturbation approach

$$\rho_{jk} = \rho_{jk}^{(0)} + \lambda\rho_{jk}^{(1)} + \lambda^2\rho_{jk}^{(2)} + \cdots, \quad (j,k = 0,1,2,3). \tag{3}$$

Here λ can be continuously evaluated between 0 and 1, while $\rho_{jk}^{(0)}$, $\rho_{jk}^{(1)}$, $\rho_{jk}^{(2)}$ are the terms of the zeroth order in $\Omega_{\rm p}$, the first order in $\Omega_{\rm p}$, the second order in $\Omega_{\rm p}$, etc. It is obvious that the atom is mostly populated in the initial ground state $|0\rangle$ in the weak-field approximation. Under this condition, we derive $\rho_{00}^{(0)} \approx 1$ and $\rho_{jk}^{(0)} \approx 0$ ($j \neq 0, k \neq 0$). The driving fields are strong fields but the probe field is very weak. Therefore, the first-order term is extremely important. Keep all of the orders

of the drive fields and the first-order terms of the probe field, the density matrix equations are obtained as

$$\mathrm{i}\dot{\rho}_{00}^{(1)} = \mathrm{i}(\gamma_1+\Gamma_t)\rho_{11}^{(1)}, \tag{4a}$$

$$\begin{aligned}\mathrm{i}\dot{\rho}_{11}^{(1)} =& -\mathrm{i}(\gamma_1+\Gamma_t)\rho_{11}^{(1)}+\mathrm{i}(\gamma_2+\Gamma_t)\rho_{22}^{(1)}\\ &+\mathrm{i}(\gamma_3+\Gamma_t)\rho_{33}^{(1)}+G_1(x,y,z)(\rho_{21}^{(1)}-\rho_{12}^{(1)})\\ &+G_2(x,y,z)(\rho_{31}^{(1)}-\rho_{13}^{(1)}),\end{aligned} \tag{4b}$$

$$\begin{aligned}\mathrm{i}\dot{\rho}_{22}^{(1)} =& -\mathrm{i}(\gamma_2+\Gamma_t)\rho_{22}^{(1)}+G_1(x,y,z)(\rho_{12}^{(1)}-\rho_{21}^{(1)})\\ &+\Omega_{mw}\rho_{32}^{(1)}-\Omega_{mw}^{*}\rho_{23}^{(1)},\end{aligned} \tag{4c}$$

$$\begin{aligned}\mathrm{i}\dot{\rho}_{33}^{(1)} =& -\mathrm{i}(\gamma_3+\Gamma_t)\rho_{33}^{(1)}+G_2(x,y,z)(\rho_{13}^{(1)}-\rho_{31}^{(1)})\\ &+\Omega_{mw}^{*}\rho_{23}^{(1)}-\Omega_{mw}\rho_{32}^{(1)},\end{aligned} \tag{4d}$$

$$\begin{aligned}\mathrm{i}\dot{\rho}_{10}^{(1)} =& -\left(\Delta_p+\mathrm{i}\frac{\gamma_1}{2}\right)\rho_{10}^{(1)}+G_1(x,y,z)\rho_{20}^{(1)}\\ &+G_2(x,y,z)\rho_{30}^{(1)}+\Omega_p,\end{aligned} \tag{4e}$$

$$\begin{aligned}\mathrm{i}\dot{\rho}_{20}^{(1)} =& -\left(\Delta_p+\Delta_1+\mathrm{i}\frac{\gamma_2+\Gamma_{23}}{2}\right)\rho_{20}^{(1)}+G_1(x,y,z)\rho_{10}^{(1)}\\ &+\Omega_{mw}\rho_{30}^{(1)},\end{aligned} \tag{4f}$$

$$\begin{aligned}\mathrm{i}\dot{\rho}_{30}^{(1)} =& -\left(\Delta_p+\Delta_2+\mathrm{i}\frac{\gamma_3+\Gamma_{32}}{2}\right)\rho_{30}^{(1)}+G_2(x,y,z)\rho_{10}^{(1)}\\ &+\Omega_{mw}^{*}\rho_{20}^{(1)},\end{aligned} \tag{4g}$$

$$\begin{aligned}\mathrm{i}\dot{\rho}_{21}^{(1)} =& -\left(\Delta_1+\mathrm{i}\frac{\gamma_2+\gamma_1+\Gamma_{23}}{2}\right)\rho_{21}^{(1)}-G_2(x,y,z)\rho_{23}^{(1)}\\ &+G_1(x,y,z)(\rho_{11}^{(1)}-\rho_{22}^{(1)})+\Omega_{mw}\rho_{31}^{(1)},\end{aligned} \tag{4h}$$

$$\begin{aligned}\mathrm{i}\dot{\rho}_{31}^{(1)} =& -\left(\Delta_2+\mathrm{i}\frac{\gamma_3+\gamma_1+\Gamma_{32}}{2}\right)\rho_{31}^{(1)}-G_1(x,y,z)\rho_{32}^{(1)}\\ &+G_2(x,y,z)(\rho_{11}^{(1)}-\rho_{33}^{(1)})+\Omega_{mw}^{*}\rho_{21}^{(1)},\end{aligned} \tag{4i}$$

$$\begin{aligned}i\dot{\rho}_{32}^{(1)} =& \left(\Delta_1-\Delta_2-\mathrm{i}\frac{\gamma_3+\gamma_2+\Gamma_{32}+\Gamma_{23}}{2}\right)\rho_{32}^{(1)}\\ &-G_1(x,y,z)\rho_{31}^{(1)}+G_2(x,y,z)\rho_{12}^{(1)}\\ &+\Omega_{mw}^{*}(\rho_{22}^{(1)}-\rho_{33}^{(1)}),\end{aligned} \tag{4j}$$

where γ_1, γ_2, γ_3, Γ_{23}, and Γ_{32} denote the decay rates from the state $|1\rangle$ to $|0\rangle$, from the state $|2\rangle$ to $|1\rangle$, from the state $|3\rangle$ to $|1\rangle$, from the state $|2\rangle$ to $|3\rangle$, and from the state $|3\rangle$ to $|2\rangle$, respectively.[40] $\Gamma_t = 2u/(\sqrt{\pi}d)$ is the transit time decay rate with the most probable speed of atoms ($u=\sqrt{2k_BT/m}$, k_B, T, and m are the Boltzmann constant, the absolute temperature, and the mass of the atom, respectively and the laser beam diameter $d = 2$ mm).[54] From Ref. [55], $\Gamma_{23} = (\Gamma_t g_2)/(g_2+g_3)$ and $\Gamma_{32} = (\Gamma_t g_3)/(g_2+g_3)$, where g_i is the degeneracy of the i-th level. In our model, $g_2 = 9$ and $g_3 = 7$. More remarkably, due to the transition from states $|3\rangle$ and $|2\rangle$ to $|0\rangle$ are nondipole, thus, the decay rates of these transitions are 0. In order to solve Eqs. (4a)–(4j), we set Ω_p, Ω_1, and Ω_2 as real, while Ω_{mw} is given as a complex parameter, i.e, $\Omega_{mw} = |\Omega_{mw}|e^{i\phi}$, ϕ named the relative phase is the phase of the microwave-driven field. Two transition ways from ground state $|0\rangle$ to excited state $|3\rangle$ can be seen in Fig. 1. The first way is $|0\rangle \overset{\Omega_p}{\to} |1\rangle \overset{\Omega_2}{\to} |3\rangle$ and the second one is $|0\rangle \overset{\Omega_p}{\to} |1\rangle \overset{\Omega_1}{\to} |2\rangle \overset{\Omega_{mw}}{\to} |3\rangle$. So, the relative phase ϕ can be explained as quantum interference resulted from these two excitation channels in the above-mentioned closed-loop structure. The atomic structure mentioned above can be realized by considering the transitions $5S_{1/2} \leftrightarrow 5P_{3/2} \leftrightarrow 5D_{5/2,3/2}$ in ^{87}Rb atom.[56] The designated levels can be selected as follows: $|0\rangle = |5S_{1/2}, F=2\rangle$, $|1\rangle = |5P_{3/2}, F=3\rangle$, $|2\rangle = |5D_{5/2}, F=4\rangle$, $|3\rangle = |5D_{3/2}, F=3\rangle$, as indicated in Fig. 2. The position-dependent probe absorption can be obtained via the heterodyne measurement of fluorescence or a standard spectroscopic method, which may be realized by the experiment proposed in Refs. [30,57]. Hence, our proposed atomic system is feasible in the practical experiment.

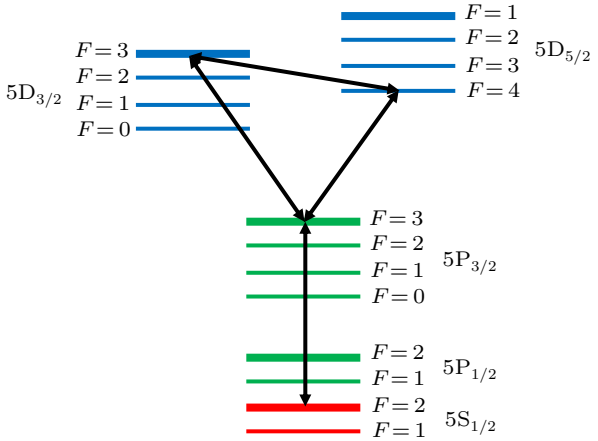


Fig. 2. Plot of possible experimental scheme with a ^{87}Rb atomic system by using the transitions $5S_{1/2} \leftrightarrow 5P_{3/2} \leftrightarrow 5D_{5/2,3/2}$.

Based on Eqs. (4a)–(4j) and the conservation of probability $\mathrm{tr}(\rho) = 1$, i.e., $\rho_{00}^{(00)}+\rho_{00}^{(1)}+\rho_{11}^{(1)}+\rho_{22}^{(1)}+\rho_{33}^{(1)} = 1$, the steady-state solutions of the first-order density matrix elements can be solved. By replacing γ_2 and γ_3 of Eq. (6) in Ref. [40] with $\gamma_2+\Gamma_{23}$ and $\gamma_3+\Gamma_{32}$, respectively, the off-diagonal density-matrix element $\rho_{10}^{(1)}$ is obtained.

The linear susceptibility of the medium can be given by

$$\chi^{(1)} = \frac{N\mu_{10}}{\varepsilon_0 E_p}\rho_{10}^{(1)} = \frac{K}{\Omega_p}\rho_{10}^{(1)}, \tag{5}$$

where $K = N|\mu_{10}|^2/(2\hbar\varepsilon_0)$, in which N represents the atom number density in the medium and ε_0 is the permittivity in free space. So, the probe absorption can be straightforwardly written as

$$\chi''^{(1)}(x,y,z) = \mathrm{Im}\left[\frac{\chi^{(1)}(x,y,z)}{K}\right]. \tag{6}$$

Owing to the fact that the cold atom experiment setup is not only complicated but also expensive, we would like to use hot atom in our work. For this reason, we have to consider how the temperature affects the 3D atom localization.[58] In the following discussion, we assume that the atom moves in

the z direction. The fields propagating along z are important to include the effect of Doppler shift. For case (i), the probe field and the standing-wave field E_z need to be considered for the effect of Doppler shift, however, the standing-wave E_z is comprised by two counter-propagating beams. As a result, there is no frequency shift in the standing-wave E_z. We only consider the Doppler shift of the probe field. We can replace the probe field detuning $\Delta_{\rm p}$ with $\Delta_{\rm p}+k_{\rm p}v$ in Eq. (5), where v is the velocity of the atom and $k_{\rm p}$ is the wave-vector of the probe field. For case (ii), we assume that the traveling-wave field G_2 propagates along the z direction, thus, the probe field detuning $\Delta_{\rm p}$ and the traveling-wave field detuning Δ_2 in Eq. (5) should be replaced with $\Delta_{\rm p}+k_{\rm p}v$ and Δ_2+k_2v, respectively. What is more, velocity dependent $\rho_{10}^{(1)}(\Delta_{\rm p}+k_{\rm p}v)$ and $\rho_{10}^{(1)}(\Delta_{\rm p}+k_{\rm p}v,\Delta_2+k_2v)$ are supposed to be integrated by considering a Maxwell–Boltzmann distribution. In a Doppler-broadened medium, we can rewrite $\rho_{10}^{(1)}$ in Eq. (5) for different cases as

$$\rho_{10}^{(1)\prime}=\left(\frac{m}{2\pi k_{\rm B}T}\right)^{\frac{1}{2}}\int_{-\infty}^{\infty}\rho_{10}^{(1)}(\Delta_{\rm p}')\,{\rm e}^{\frac{-mv^2}{2k_{\rm B}T}}\,{\rm d}v, \tag{7a}$$

$$\rho_{10}^{(1)\prime\prime}=\left(\frac{m}{2\pi k_{\rm B}T}\right)^{\frac{1}{2}}\int_{-\infty}^{\infty}\rho_{10}^{(1)}(\Delta_{\rm p}',\Delta_2')\,{\rm e}^{\frac{-mv^2}{2k_{\rm B}T}}\,{\rm d}v, \tag{7b}$$

where $\Delta_{\rm p}'=\Delta_{\rm p}+k_{\rm p}v$ and $\Delta_2'=\Delta_2+k_2v$. The wave-vectors $k_{\rm p}$ and k_2 are $2\pi\times12816.55$ cm^{-1} and $2\pi\times12883.28$ cm^{-1}, respectively.[59]

It is obvious that the probe absorption is dependent on the parameters of the system, such as the field intensity, the field detuning, and the temperature of the atom. The probe absorption is related to the position-dependent Rabi frequencies $G_1(x,y,z)$ and $G_2(x,y,z)$. In addition, the probe absorption reflects the conditional position probability distribution of the atom. So, we can obtain the information of atom localization when it moves through the standing-wave fields by measuring the probe absorption. The atom can be precisely localized by adjusting the tunable parameters of the system.

3. Numerical results and discussion

In this section, we will investigate the conditional position probability distribution of the atom in 3D space by doing numerical calculations based on Eq. (7) and discuss these numerical results. In order to achieve high-precision 3D atom localization, we study the effects of the system parameters on the atom localization via considering two cases. For case (i), both $G_1(x,y,z)$ and $G_2(x,y,z)$ are the standing-wave fields, i.e., $G_1(x,y,z)=\Omega_1[\sin(k_1x)+\sin(k_1y)]$ and $G_2(x,y,z)=\Omega_2\sin(k_2z)$; for case (ii), $G_1(x,y,z)$ is a standing-wave field composed by three orthogonal standing-wave fields, but $G_2(x,y,z)$ is assumed as a traveling-wave field, i.e., $G_1(x,y,z)=\Omega_1[\sin(k_1x)+\sin(k_1y)+\sin(k_1z)]$ and $G_2(x,y,z)=\Omega_2$. In both cases, $G_1(x,y,z)$ and $G_2(x,y,z)$ are used to couple the transitions $|1\rangle\leftrightarrow|2\rangle$ and $|1\rangle\leftrightarrow|3\rangle$, respectively. We emphasize that all the parameters applied in this paper are in units of γ, which is supposed to be on the order of $2\pi\times3$ MHz for ^{87}Rb, besides, $\gamma_1=2\gamma,\gamma_2=\gamma_3=0.32\gamma$, $k_{\rm p}=0.427\gamma$, and $k_2=0.429\gamma$.[40,59]

However, there are many controllable parameters in this model. The issue can be solved via the following steps. First of all, we assume that there is no detuning in the model. Secondly, considering that the microwave field intensity is equal to, less than, and greater than the standing-wave field intensity, we then conclude which condition is beneficial for localizing the atom; Thirdly, the intensities of the fields are finely tuned for achieving high-precision atom localization. Fourthly, after setting the standing-wave field intensity and the microwave field intensity to the above values, we consider that the probe field detuning is equal to, less than, and greater than the standing-wave field detuning, and then conclude which case is beneficial to local the atom. Finally, the detunings of the fields are finely tuned for achieving high-precision atom localization. In the following study, the system parameters are set by the above steps.

3.1. Case (i)

The first case is that both $G_1(x,y,z)$ and $G_2(x,y,z)$ are standing-wave fields. In the following, we give the numerical results about the probe absorption with different parameters.

The probe absorption versus the positions (kx,ky,kz) for different intensities of the fields (Ω_1, Ω_2, and $\Omega_{\rm mw}$) are plotted in Fig. 3. Figures 3(a) and 3(b) present that the probe absorption spreads across all subspaces, thus, the location information of the atom is ambiguous. The probe absorption is distributed in four subspaces with a small diameter of sphere-like structure, as shown in Fig. 3(c). From Figs. 3(a) and 3(b), one can find the precision of atom localization is not changed when the microwave field intensity decreases. Direct comparison of Figs. 3(a) and 3(c) indicates that the precision of atom location will increase as the intensity of the standing-wave field decreases. It is noteworthy that the variation of the precision of atom localization with the standing-wave field intensity is different with that of the microwave field.

Figure 4 illustrates the effect of the standing-wave field detuning (Δ_1, Δ_2), the probe field detuning ($\Delta_{\rm p}$), and the temperature of the atom on the 3D atom localization. It is obvious that the probe absorption distribution in Fig. 4(b) is similar to that in Fig. 4(a). From Fig. 4(c), the atom position information cannot be obtained because the probe absorption is distributed in four subspaces. Comparing Fig. 4(a) with Figs. 4(b) and 4(c) respectively, one can conclude that the precision of atom localization is improved when the probe field detuning increases. It is clear that the system parameters used in Fig. 4(c)

are the best choice for high-precision atom localization when the temperature of the atom is closed to the room temperature. As a consequence, the system parameters used in Fig. 4(d) are the same as those in Fig. 4(c) when we research the effect of the temperature of the atom, except that the temperature of the atom is equal to 323 K. The results in Figs. 4(c) and 4(d) show that the precision of atom localization is improved with the increase of the absolute temperature.

Table 1. The system parameters for high-precision atom localization in both cases.

	$\Omega_{1,2}$	$\Omega_{\rm mw}$	$\Delta_{1,2}$	$\Delta_{\rm p}$
Without detuning	5γ	20γ	0	0
With detuning	5γ	20γ	5γ	30γ

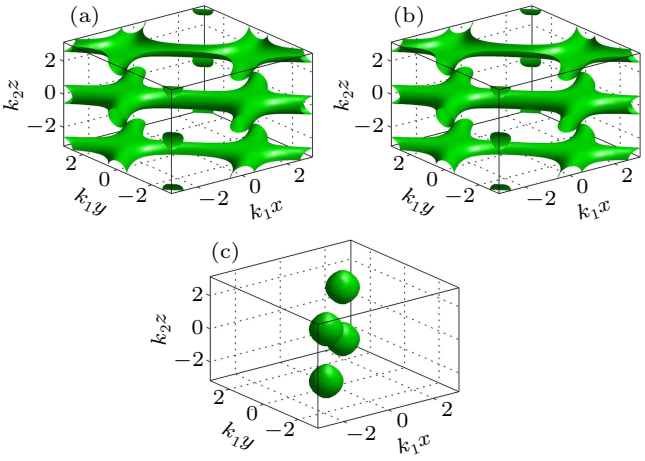


Fig. 3. Isosurface plots for the probe absorption $\chi''^{(1)}$ versus positions (kx, ky, kz) for different values of the driving field Ω_1, Ω_2, and $\Omega_{\rm mw}$. (a) $\Omega_1 = \Omega_2 = 20\gamma$, $\Omega_{\rm mw} = 20\gamma$; (b) $\Omega_1 = \Omega_2 = 20\gamma$, $\Omega_{\rm mw} = 5\gamma$; (c) $\Omega_1 = \Omega_2 = 5\gamma$, $\Omega_{\rm mw} = 20\gamma$. The other parameters used are $\phi = 0$, $\gamma = 1$, $\gamma_1 = 2\gamma$, $\gamma_2 = \gamma_3 = 0.32\gamma$, $\Delta_1 = \Delta_2 = 0$, $\Delta_{\rm p} = 0$, $k_{\rm p} = 0.427\gamma$, and $T = 298$ K.

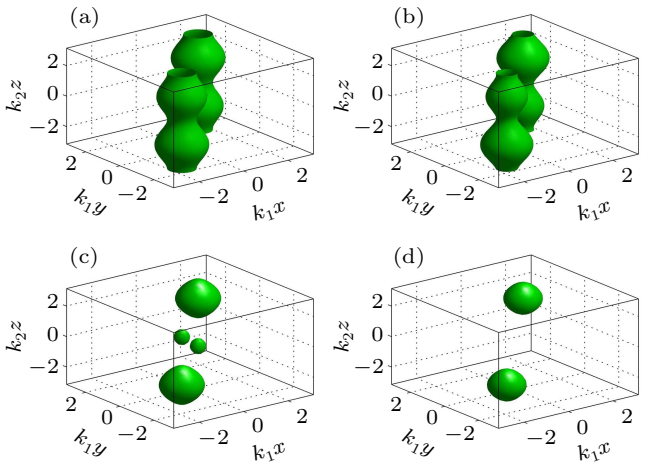


Fig. 4. Isosurface plots for the probe absorption $\chi''^{(1)}$ versus positions (kx, ky, kz) for different values of the detuning Δ_1, Δ_2, and $\Delta_{\rm p}$. (a) $\Delta_1 = \Delta_2 = 5\gamma$, $\Delta_{\rm p} = 5\gamma, T = 298$ K; (b) $\Delta_1 = \Delta_2 = 30\gamma$, $\Delta_{\rm p} = 5\gamma, T = 298$ K; (c) $\Delta_1 = \Delta_2 = 5\gamma$, $\Delta_{\rm p} = 30\gamma, T = 298$ K; (d) $\Delta_1 = \Delta_2 = 5\gamma$, $\Delta_{\rm p} = 30\gamma, T = 323$ K. The other parameters used are $\phi = 0$, $\gamma = 1$, $\gamma_1 = 2\gamma$, $\gamma_2 = \gamma_3 = 0.32\gamma$, $\Omega_1 = \Omega_2 = 5\gamma$, $\Omega_{\rm mw} = 20\gamma$, $k_{\rm p} = 0.427\gamma$, and $k_2 = 0.429\gamma$.

3.2. Case (ii)

The second case is that $G_1(x, y, z)$ is a standing-wave field in the x, y, and z direction, while $G_2(x, y, z)$ is a traveling-wave field with the intensity Ω_2 independent of the position. The following illustrations display the numerical results of 3D atom localization with different values of the system parameters.

The effects of the intensities of the fields (Ω_1, Ω_2, and $\Omega_{\rm mw}$) on the spatial distribution of the atom are plotted in Fig. 5. Clearly, the information of atom position is ambiguous in Figs. 5(a) and 5(b), which is attributed to the fact that the probe absorption is distributed in different subspaces. In Fig. 5(c), the atom is localized in the subspace (kx, ky, kz) and $(-kx, -ky, -kz)$, consequently, the probability of the atom in such case is $\lambda/2$ within one period of standing-wave fields. There is no doubt that decreasing the microwave field intensity is not helpful to 3D atom localization by comparing Fig. 5(a) with Fig. 5(b), which is in accord with the result of the cold atom when the probe detuning is not tuned to zero.[52] Comparing Fig. 5(a) with Fig. 5(c), one can conclude that the standing-wave field intensity should be tuned as small as possible for improving the precision of atom localization when $\Omega_{\rm mw} = 20\gamma$.

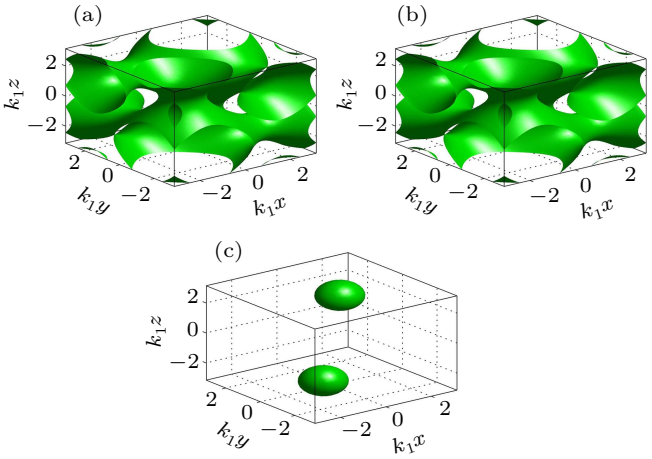


Fig. 5. Isosurface plots for the probe absorption $\chi''^{(1)}$ versus positions (kx, ky, kz) for different values of the driving field Ω_1, Ω_2, and $\Omega_{\rm mw}$. (a) $\Omega_1 = \Omega_2 = 20\gamma$, $\Omega_{\rm mw} = 20\gamma$; (b) $\Omega_1 = \Omega_2 = 20\gamma$, $\Omega_{\rm mw} = 5\gamma$; (c) $\Omega_1 = \Omega_2 = 5\gamma$, $\Omega_{\rm mw} = 20\gamma$. The system parameters used are the same as those in Fig. 3.

Figure 6 shows the influence of the standing-wave field detuning (Δ_1, Δ_2), the probe field detuning ($\Delta_{\rm p}$), and the temperature on the 3D atom localization. Figure 6(d) shows clearly that the atom can be localized with a high precision, because the probe absorption just appears in a subspace (kx, ky, kz). As indicated in Figs. 6(a) and 6(b), the probe absorption spreads across two subspaces. Accordingly, the location information of the atom is ambiguous in Figs. 6(a) and 6(b). Comparing Fig. 6(a) with Figs. 6(b) and 6(c), respectively, one can find that increasing the detuning of the probe

field will be beneficial to localizing atom with a high precision, which is in accord with the results of the cold atom when the microwave intensity is set to zero or not.[52] The same as the result of Fig. 4(d), the precision of atom localization is changed obviously when the temperature of the atom is equal to 323 K.

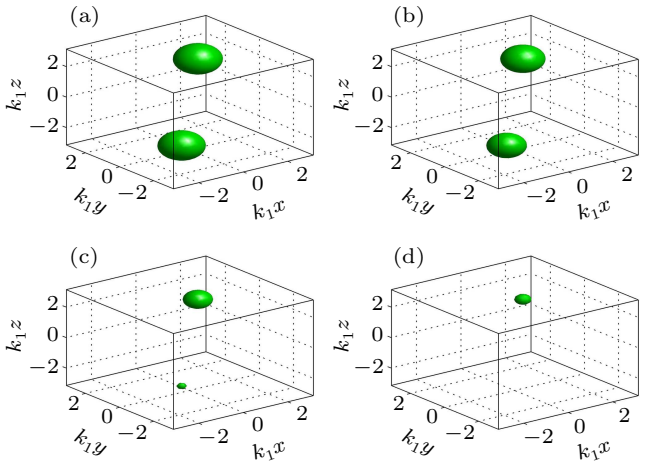


Fig. 6. Isosurface plots for the probe absorption $\chi''^{(1)}$ versus positions (kx, ky, kz) for different values of the detuning Δ_1, Δ_2, and Δ_p. (a) $\Delta_1 = \Delta_2 = 5\gamma$, $\Delta_p = 5\gamma$, $T = 298$ K; (b) $\Delta_1 = \Delta_2 = 30\gamma$, $\Delta_p = 5\gamma$, $T = 298$ K; (c) $\Delta_1 = \Delta_2 = 5\gamma$, $\Delta_p = 30\gamma$, $T = 298$ K; (d) $\Delta_1 = \Delta_2 = 5\gamma$, $\Delta_p = 30\gamma$, $T = 323$ K. The system parameters used are the same as those in Fig. 4.

In both cases, the intensities of the standing-wave field and the microwave field should be set as $\Omega_1 = \Omega_2 = 5\gamma$ and $\Omega_{mw} = 20\gamma$, respectively, for high-precision atom localization when the standing-wave detuning and the probe detuning are tuned to zeros. However, if the standing-wave detuning and the probe detuning are not tuned to zeros, the standing-wave and the probe detuning should be set as $\Delta_1 = \Delta_2 = 5\gamma$ and $\Delta_p = 30\gamma$ in both cases. Table 1 lists the values of the above parameters for localizing the atom with a high precision at room condition in both cases. There is an obvious precision change when the temperature of the atom is adjusted from 298 K to 323 K in both cases, so, high-precision atom localization can be got via increasing the temperature of the atom in our model. It is worth noting that the temperature should not be too high as the collision effects cannot be negligible even at $T = 333$ K.[55]

4. Conclusions

In this paper, we show how to solve the problem that there are many controllable parameters in a model. And we have investigated the influences of the system parameters, such as the intensity of the laser fields, the detuning of the fields, and the temperature on 3D atom localization by probe absorption in a hot atomic system. We find that the atom can be localized in a subspace when the temperature is equal to 323 K by setting the system parameters at the appropriate values, which has been achieved in cold atom. However, the experiment for the cold atom localization is complicated. Besides, we conclude that the atom cannot be localized in a subspace when $G_1(x, y, z)$ and $G_2(x, y, z)$ corresponding to the standing-wave fields for the probe absorption shows a symmetrical distribution. The best precision is close to 0.1λ as shown in Fig. 6(d). Tailoring the luminescence spectrum, which can be achieved by controlling the position of the atom, has an important application in the photonic crystal and single molecule spectroscopy.[60] As a consequence, our study not only simplify the experiment configuration but also is useful for atom lithography, tailoring luminescence spectrum,[61] and the high-precision measurement of the center-of-mass wave function of moving atoms.[62]

References

[1] Metcalf H and Van der Stratenb P 1994 *Phys. Rep.* **244** 203
[2] Phillips W D 1998 *Rev. Mod. Phy.* **70** 721
[3] Gorshkov A V, Jiang L, Greiner M, Zoller P and Lukin M D 2008 *Phys. Rev. Lett.* **100** 093005
[4] Mompart J, Ahufinger V and Birkl G 2009 *Phys. Rev. A* **79** 053638
[5] Kapale K T, Qamar S and Zubairy M S 2003 *Phys. Rev. A* **67** 023805
[6] Evers J, Qamar S and Zubairy M S 2007 *Phys. Rev. A* **75** 053809
[7] Johnson K S, Thywissen J H, Dekker N H, Berggren K K, Chu A P, Younkin R and Prentiss M 1998 *Science* **280** 1583
[8] Collins G P 1996 *Phys. Today* **49** 18
[9] Wu Y, Yang X and Sun C 2000 *Phys. Rev. A* **62** 063603
[10] Wu Y and Côté R 2002 *Phys. Rev. A* **65** 053603
[11] Born M and Wolf E 1999 *Principles of Optics* (Cambridge: Cambridge University Press) p. 517
[12] Kunze S, Rempe G and Wilkens M 1994 *Epl* **27** 115
[13] Storey P, Collett M and Walls D 1992 *Phys. Rev. Lett.* **68** 472
[14] Storey P, Collett M and Walls D 1993 *Phys. Rev. A* **47** 405
[15] Storey P, Sleator T, Collett M and Walls D 1994 *Phys. Rev. A* **49** 2322
[16] Thomas J E 1990 *Phys. Rev. A* **42** 5652
[17] Stokes K D, Schnurr C, Gardner J R, Marable M, Welch G R and Thomas J E 1991 *Phys. Rev. Lett.* **67** 1997
[18] Gardner J R, Marable M L, Welch G R and Thomas J E 1993 *Phys. Rev. Lett.* **70** 3404
[19] Jiao Y C, Han X X, Yang Z W, Zhao J M and Jia S T 2016 *Chin. Phys. Lett.* **33** 123201
[20] Yan D, Wang B B, Bai W J, Liu B, Du X G and Ren C N 2019 *Acta Phys. Sin.* **68** 084203 (in Chinese)
[21] Jia Y, Chen X H, Zhang H, Zhang L J, Xiao L T and Jia S T 2018 *Acta Phys. Sin.* **67** 213201 (in Chinese)
[22] Liu H, Qin L G, Tian L J and Ma H Y 2019 *Chin. Phys. B* **28** 108502
[23] Hao L P, Xue Y M, Fan J B, Jiao Y C, Zhao J M and Jia S T 2019 *Chin. Phys. B* **28** 053202
[24] Paspalakis E and Knight P L 2001 *Phys. Rev. A* **63** 065802
[25] Kapale K T and Zubairy M S 2006 *Phys. Rev. A* **73** 023813
[26] Ghafoor F, Qamar S and Zubairy M S 2002 *Phys. Rev. A* **65** 043819
[27] Xu J and Hu X M 2007 *Phys. Rev. A* **76** 013830
[28] Nha H, Lee J H, Chang J S and An K 2002 *Phys. Rev. A* **65** 033827
[29] Liu C, Gong S, Cheng D, Fan X and Xu Z 2006 *Phys. Rev. A* **73** 025801
[30] Proite N A, Simmons Z J and Yavuz D D 2011 *Phys. Rev. A* **83** 041803
[31] Gardner J R, Marable M L, Welch G R and Thomas J E 1993 *Phys. Rev. Lett.* **70** 3404
[32] Guidoni L and Verkerk P 1998 *Phys. Rev. A* **57** R1501
[33] Qamar S, Zhu S Y and Zubairy M S 2000 *Opt. Commun.* **176** 409
[34] Rahmatullah and Qamar S 2013 *Phys. Lett. A* **377** 1587
[35] Wan R G, Kou J, Jiang L, Jiang Y and Gao J Y 2011 *J. Opt. Soc. Am. B* **28** 10
[36] Ivanov V S and Rozhdestvensky Y V 2010 *Phys. Rev. A* **81** 033809
[37] Wan R G, Kou J, Jiang L, Jiang Y and Gao J Y 2011 *J. Opt. Soc. Am. B* **28** 622
[38] Li J H, Yu R, Liu M, Ding C L and Yang X X 2011 *Phys. Lett. A* **375** 3978
[39] Ding C L, Li J H, Zhan Z M and Yang X X 2011 *Phys. Rev. A* **83** 063834

[40] Ding C L, Li J H, Yang X X, Zhang D and Xiong H 2011 *Phys. Rev. A* **84** 043840
[41] Ding C L, Li J H, Yu R, Hao X Y and Wu Y 2012 *Opt. Express* **20** 7870
[42] Wang Z P and Yu B L 2014 *J. Opt. Soc. Am. B* **31** 565
[43] Jin L L, Sun H, Niu Y P, Jin S Q and Gong S Q 2009 *J. Mod. Opt.* **56** 805
[44] Zhang W T and Li T B 2006 *Chin. Phys. Lett.* **23** 2952
[45] Wang Z P, Yu B L, Zhu J, Cao Z G, Zhen S L, Wu X Q and Xu F 2012 *Ann. Phys.* **327** 1132
[46] Rahmatullah and Qamar S 2014 *Phys. Lett. A* **378** 684
[47] Qi Y H, Zhou F X, Huang T, Niu Y P and Gong S Q 2012 *J. Mod. Opt.* **59** 1092
[48] Ivanov V S, Rozhdestvensky Y V and Suominen K A 2014 *Phys. Rev. A* **90** 063802
[49] Song F, Chen J Y, Wang Z P and Yu B L 2018 *Front. Phys.* **13** 134208
[50] Zhu Z H, Chen A X, Liu S P and Yang W X 2016 *Phys. Lett. A* **380** 3956
[51] Hamedi H R and Mehamannavaz M R 2016 *J. Opt. Soc. Am. B* **33** 41
[52] Mao Y S and Wu J C 2017 *J. Opt. Soc. Am. B* **34** 1070
[53] Meystre P and Sargent III M 1999 *Elements of Quantum Optics* (Berlin: Springer-Verlag) p. 144
[54] Kang H J and Noh H R 2017 *Opt. Express* **25** 21762
[55] Sagle J, Namiotka R K and Huennekens J 1995 *J. Phys. B: At. Mol. Opt. Phys.* **29** 2629
[56] Noh H R and Moon H S 2011 *Opt. Express* **19** 11128
[57] Chang J T, Evers J and Zubairy M S 2006 *Phys. Rev. A* **74** 043820
[58] Rahmatullah, Chuang Y L, Lee R K and Qamar S 2018 *Laser Phys. Lett.* **15** 035202
[59] Steck D A 2019 *Rubidium* 87*D line data*, available online at [http://steck.us/alkalidata]
[60] Wang X H, Gu B Y, Wang R Z and Xu H Q 2003 *Phys. Rev. Lett.* **91** 113904
[61] Wang D W, Zhou H T, Guo M J, Zhang J X, Evers J and Zhu S Y 2013 *Phys. Rev. Lett.* **110** 093901
[62] Zhu Z H, Yang W X, Xie X T, Liu S S, Liu S P and Lee R K 2016 *Phys. Rev. A* **94** 013826